atmosphere

MDPI

Article

Snow Avalanche Susceptibility Mapping of Transportation Corridors Based on Coupled Certainty Factor and Geodetector Models

Jie Liu [1,2,3], Xiliang Sun [1,2,3], Qiang Guo [4], Zhiwei Yang [2,3], Bin Wang [2,3], Senmu Yao [2,3,5], Haiwei Xie [1] and Changtao Hu [1,2,3,*]

[1] School of Transportation and Logistics Engineering, Xinjiang Agricultural University, Urumqi 830052, China; hfutliujie@163.com (J.L.); 320222586@xjau.edu.cn (X.S.); xiehaiwei@xjau.edu.cn (H.X.)
[2] Xinjiang Key Laboratory for Safety and Health of Transportation Infrastructure in Alpine and High-Altitude Mountainous Areas, Urumqi 830006, China; yangzhiwei19@mails.ucas.ac.cn (Z.Y.); wangbin13245@126.com (B.W.); 107552204581@stu.xju.edu.cn (S.Y.)
[3] Xinjiang Transport Planning Survey and Design Institute Co., Ltd., Urumqi 830006, China
[4] Xinjiang Uygur Autonomous Region Traffic Construction Administration, Urumqi 830049, China; xjguoqiang2024@163.com
[5] College of Civil Engineering and Architecture, Xinjiang University, Urumqi 830046, China
* Correspondence: xj11992023@163.com

Abstract: Avalanche susceptibility assessment is a core aspect of regional avalanche early warning and risk analysis and is of great significance for disaster prevention and mitigation on proposed highways. Using sky–ground integration investigation, 83 avalanche points within the G219 Wen Quan to Horgos transportation corridor were identified, and the avalanche hazard susceptibility of the transportation corridor was partitioned using the certainty factor (CF) model and the coupled coefficient of the certainty factor–Geodetector (CF-GD) model. The CF model analysis presented nine elements of natural conditions which influence avalanche development; then, by applying the Geodetector for each of the factors, a weighting coefficient was given depending on its importance for avalanche occurrence. The results demonstrate the following: (1) According to the receiver operating characteristic (ROC) curve used to verify the accuracy, the area under the ROC curve (AUC) value for the CF-GD coupled model is 0.889, which is better than the value of 0.836 of the CF model's evaluation accuracy, and the coupled model improves the accuracy by about 6.34% compared with the single model, indicating that the coupled model is more accurate. The results provide avalanche prevention and control recommendations for the G219 Wen Quan to Horgos transportation corridor. (2) The slope orientation, slope gradient, and mean winter temperature gradient are the main factors for avalanche development in the study area. (3) The results were validated based on the AUC values. The AUCs of the CF-GD coupled model and the CF model were 0.889 and 0.836, respectively. The accuracy of the coupled model was improved by about 6.34% compared to the single model, and the coupled CF-GD model was more accurate. The results provide avalanche control recommendations for the G219 Wen Quan to Horgos transportation corridor.

Keywords: G219 traffic corridor; snow avalanche; snow avalanche susceptibility; CF; CF-GD

Citation: Liu, J.; Sun, X.; Guo, Q.; Yang, Z.; Wang, B.; Yao, S.; Xie, H.; Hu, C. Snow Avalanche Susceptibility Mapping of Transportation Corridors Based on Coupled Certainty Factor and Geodetector Models. *Atmosphere* **2024**, *15*, 1096. https://doi.org/10.3390/atmos15091096

Academic Editor: Tin Lukić

Received: 10 August 2024
Revised: 5 September 2024
Accepted: 6 September 2024
Published: 9 September 2024

1. Introduction

The cryosphere is one of the five major portions of the climate system. The ongoing retreat of the global cryosphere has been affecting human societies and has caused a series of snow- and ice-related disasters (SIRDs). SIRDs mainly occur in high mountainous areas with middle–low latitude and permafrost regions with high latitude, and are accompanied with the increasing frequency of glacier, snow, and glacier lake outburst flood-related disasters and an expanding range of freeze–thaw disasters. These disasters have caused tremendous damage and impact [1–4].

Among these, avalanches are one of the most intensely active geologic hazards in the cryosphere and are characterized by suddenness, potentiality, rapid movement, destructiveness, and difficulty in prediction [5–7]. Avalanches often block transportation corridors, which threaten the safety of people's lives and property and affect the economic development of people living in mountainous areas [8–10]. In March 2008, an avalanche induced by strong winds destroyed construction camps and buried construction tunnels in the Guozigou region of the Ili Kazakh Autonomous Prefecture in Xinjiang, resulting in the deaths of 16 people, injuries to 8 individuals, and the loss of the natural gas supply. In December 2010, an avalanche triggered by heavy snowfall impacted passing vehicles and cut off roads in the G218 Tianshan section, killing two people and trapping thousands of vehicles in the mountainous area. In April 2019, an avalanche buried a mountain road in Urumqi's Nanshan Scenic area, injuring and trapping 10 people [11].

To study the hazards and characteristics of avalanches, scholars have carried out modeling studies on avalanches [12–15]; however, the conditions for training these models are harsh and cannot be satisfied for different regions. Faced with the threat of avalanche hazards, a regional avalanche susceptibility assessment can help identify avalanche hazards early [6,16]. Avalanche susceptibility assessments are an important part of regional avalanche warning and risk analysis. The results can provide support for avalanche monitoring and early warning, and in engineering, can provide a basis for avalanche prevention and control, which can reduce the risk and losses associated with avalanches.

Remote sensing (RS) and geographic information system (GIS) technologies are being used together to assess geohazards [17], and the application of '2S' technology in analyzing hydrological and geological hazards [18,19]. Methods for evaluating the susceptibility to geologic hazards are constantly being updated, theoretical systems are more complete, and evaluation methods have changed from qualitative analysis to objective quantitative analysis [20]. Qualitative analysis is too subjective and is susceptible to human interference. Quantitative avalanche susceptibility assessment methods mainly include machine learning methods [21] such as multivariate discriminant analysis [22], decision trees [23], and support vector machines [24]. Machine learning methods are more frequently used and more complex in terms of their iterative operations. It has been found that mathematical and statistical methods such as the certainty factor (CF) [11], the informativeness model [25], and Geodetector [26] can yield quantitative conclusions, and they have been widely used because they are easy for researchers to calculate and analyze. Li Yimin et al. [27] used a deterministic coefficient model to establish a mudslide disaster susceptibility evaluation system for Lushui City, and the accuracy of their susceptibility evaluation results reached 81.99%. Dou Jie et al. [28] used a deterministic coefficient model to assess landslide susceptibility in the Nakagoshi area of the Niigata Prefecture, central Japan, and their results showed that the area under the remote operator characteristic (ROC) curve (AUC) value of this model reached 0.82, indicating that it is highly accurate. Sujatha et al. [29] assessed the landslide susceptibility of the Kodaikkanal Tevankarai Ar watershed, India, based on the coefficient of determination model and categorized the landslide susceptibility map into five classes. They found that 93.32% of the study area was in the low susceptibility category and 6.34% was located in the high and very high susceptibility zones. Jia W et al. [30] used a Geodetector model, combined with spatial interpolation and index extraction techniques, to reveal the driving factors of geohazards and reported that the strength of the association between seven influencing factors and geohazards in the study area varied significantly. Liao et al. [31] used a probe to identify the main drivers of avalanches in Ganzhou City, China, and they showed that the main drivers of avalanche erosion were rainfall erosion, elevation, and land use. Du Yuchen et al. [32] carried out a susceptibility evaluation of the mudslide susceptibility in the Anning River Basin using a coupled model of deterministic coefficients and Geodetectors, and the results of their evaluation exhibited a high degree of accuracy.

A single evaluation model or method has some limitations [33]. The deterministic coefficient model can quickly analyze the weight of each factor, but there is a sensitiv-

ity of each factor to the evaluation of susceptibility. In contrast, the probe detects the relationship between the influencing factors and the geographic phenomena without any linear assumptions, and gives a weighting coefficient for each factor that depends on its importance for avalanche occurrence, which can bypass the influence of subjective factors on the evaluation results. By coupling probes, the shortcomings of a single CF model can be compensated.

According to data from meteorological stations, the snow accumulation period in the G219 Wen Quan to Khorgos transportation corridor is more than 5 months long, and avalanche disasters pose a serious threat to the transportation corridor. There are few researchers working in this area at present. The coupled certainty factor–Geodetector (CF-GD) model is highly accurate but lacks applicability in avalanche hazard susceptibility assessment.

Motivated by this research gap, in this study, avalanches along the transportation corridor from G219Wen Quan to Horgos in Xinjiang were taken as the research object, and a coupled CF-GD model was established to calculate and optimize the hierarchical affiliation and factor sensitivity of avalanche susceptibility evaluation factors by adopting a joint sky–ground investigation and an observational data-driven model to improve the accuracy of avalanche disaster susceptibility evaluations. Using the coupled model, the evaluation of avalanche disaster susceptibility in the study area was carried out, and the evaluation accuracy was verified and analyzed using the field investigation data to provide a reference for the study of avalanche disaster prevention and control in the study area and development of early warning decision-making schemes.

The main contributions of this study are threefold. First, the coefficient of the certainty factor and Geodetector models were applied to the assessment of avalanche hazards, and the prediction accuracies of the coupled model and the single model were compared. Second, the conditions favorable to avalanche development in the traffic corridor were analyzed. Finally, the snow avalanche susceptibility of the transportation corridors was mapped.

2. Study Area and Data Sources

2.1. Study Area

The G219Wen Quan to Khorgos transportation corridor (hereafter referred to as the transportation corridor) is oriented in the southeast direction in the Beizhentai Mountains, a branch of Western Tien Shan, and is bordered by Sayram Lake in the east and the Boroko Nu Mountains (Figure 1a). The study area is the geomorphological demarcation line between the Bortala Valley and the pre-hills and plains of the Khorgos Mountains. The topography is high in the center and low on both ends and is characterized by severe surface cuts, steep mountains, large changes in the topographic relief, and geomorphology that is characterized by low to medium mountains and river valleys [34]. The elevation is 1.4–3.5 km and the slope gradient is between 30 and 60° (Figure 1b). The vertical geographic distribution structure of the mountain system is obvious, and the data from the meteorological stations in the study area show that the snow depth can reach up to 1.6 m, so the meteorological and topographic conditions create favorable conditions for avalanche development.

2.2. Data Processing

2.2.1. Avalanche Inventory

Since 2023, measured data on avalanche hazard characteristics such as the topography, geomorphology, snow characteristics, and meteorological conditions in the study area have been obtained using unmanned aerial vehicle (UAV) remote sensing, on-site surveys, and fixed-point observations at meteorological stations. Through sky–ground integration and synergistic investigation, it was found that there are multiple avalanche hazard points in the study area, and the avalanches within the corridors are mostly gully avalanches, as well as a small portion of slope avalanches (Figure 2b,c). A total of 83 avalanche points were identified in the transportation corridor.

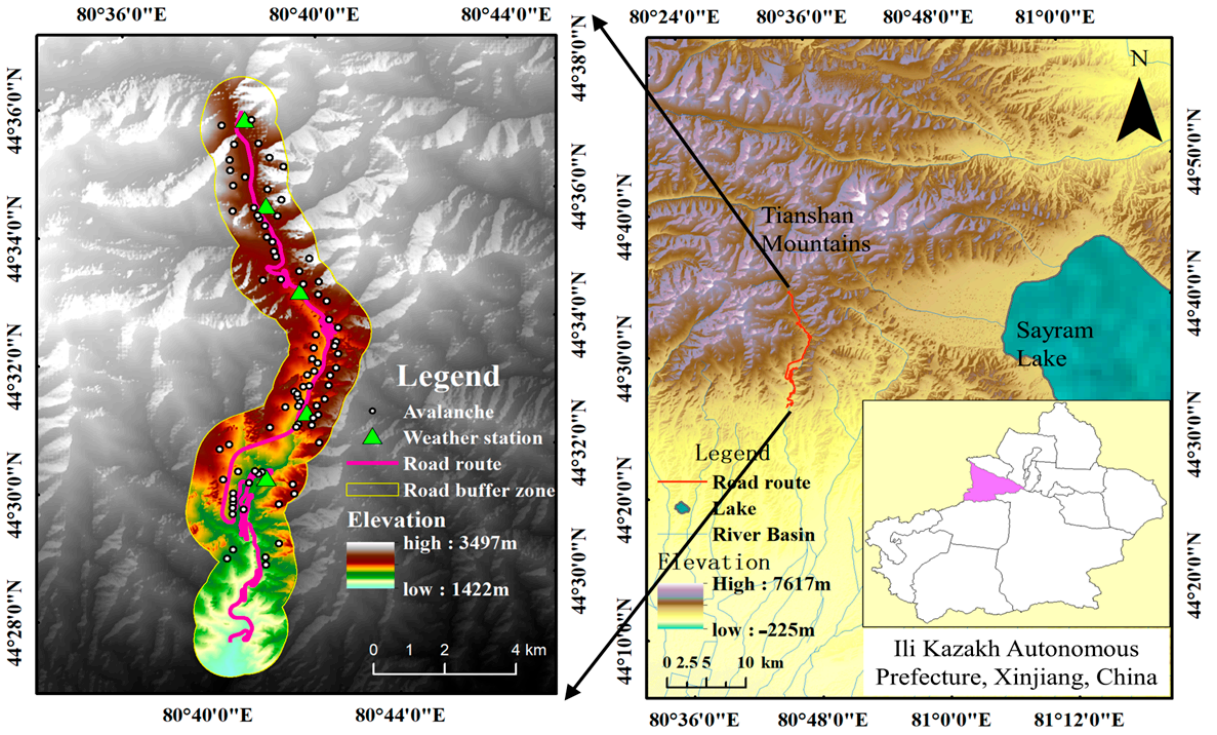

(**a**)

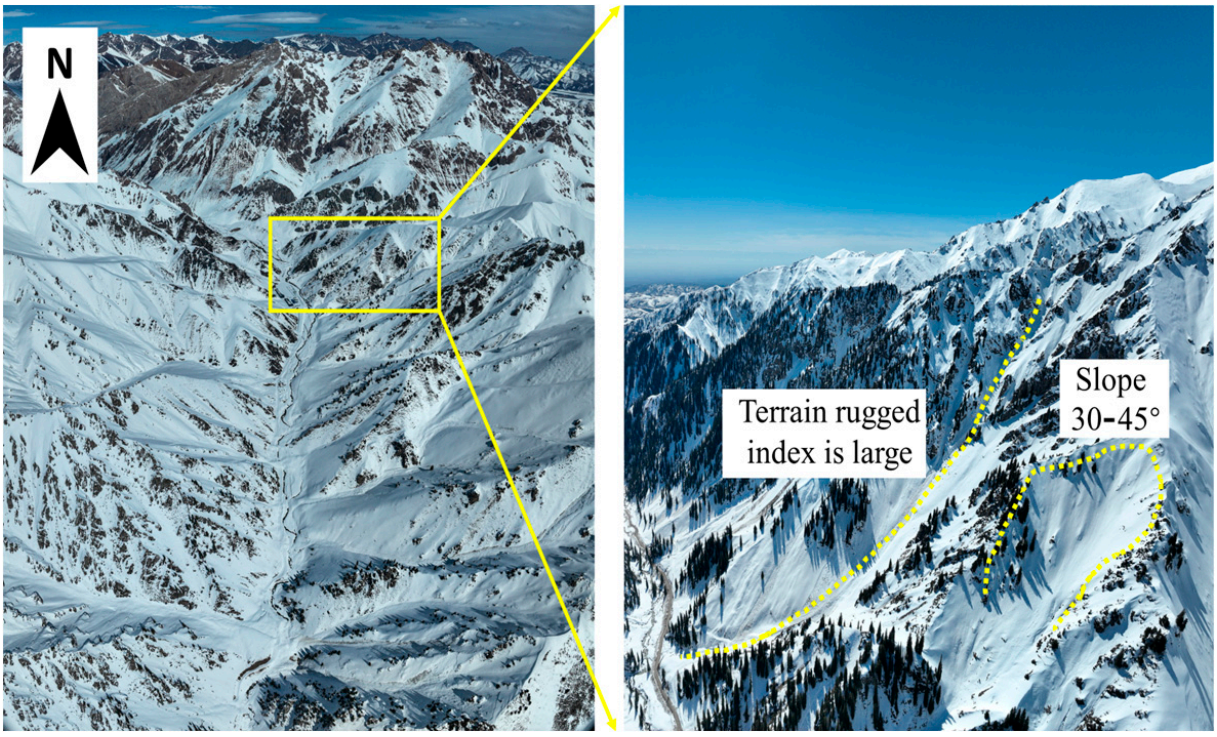

(**b**)

Figure 1. Sketch map of the study area: (**a**) map showing the location of the study area; (**b**) topographic map of the transportation corridor.

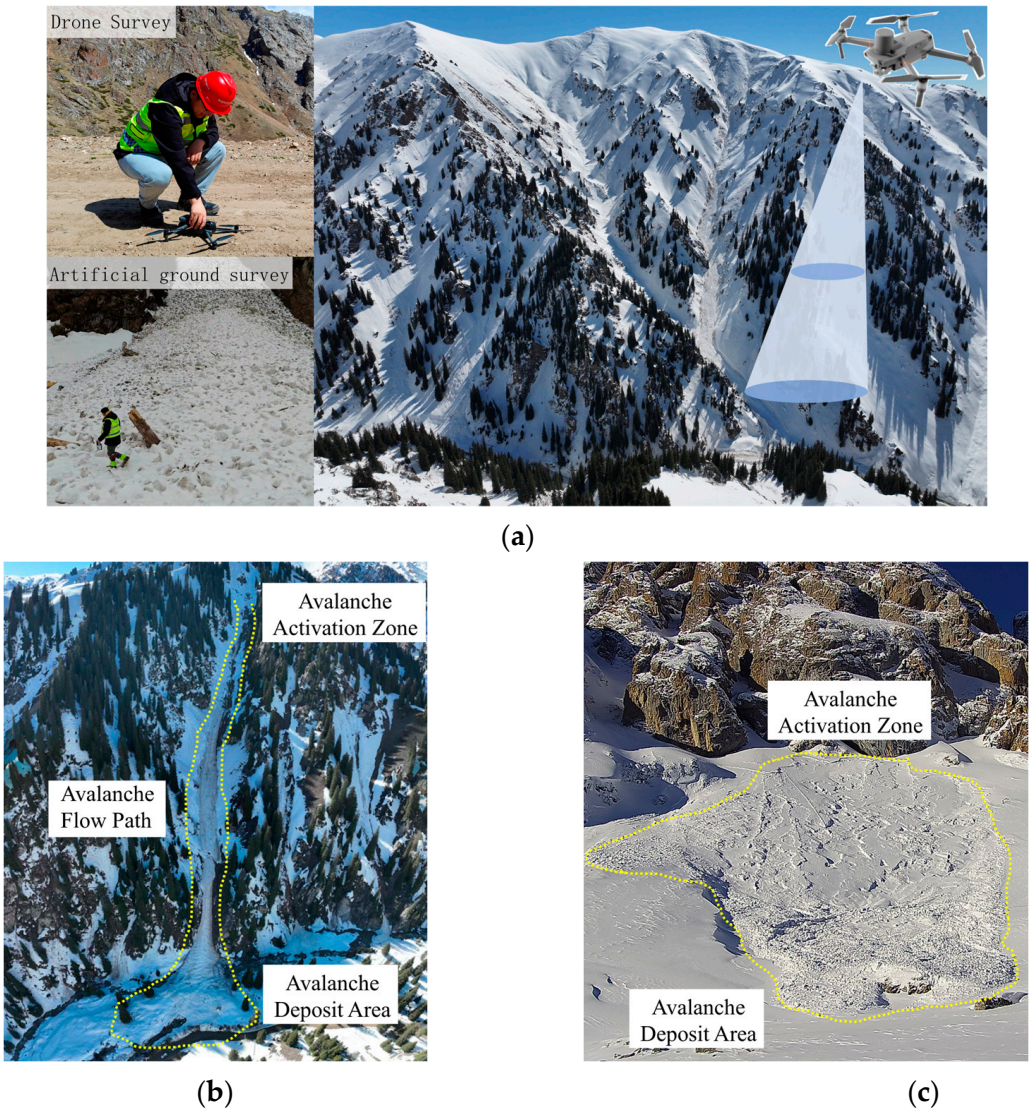

Figure 2. Visit to transportation corridor to investigate avalanche distribution in 2024: (**a**) sky–ground integrated collaborative investigation; (**b**) grooved avalanche; (**c**) slope-based avalanches.

2.2.2. Geographic Information Data

The elevation, terrain relief, surface cuts, ground roughness, slope, and slope direction initial state factors were extracted using ArcGIS-10.8 software and a digital elevation model (DEM) with a resolution of 12.5 m downloaded from the Geospatial Data Cloud, we accessed it on 5 October 2023. (https://www.gscloud.cn/) [35].

2.2.3. Meteorological Data

Based on meteorological data from five meteorological stations along the corridor, the average monthly winter temperature gradient, average winter snow depth, and average winter wind speed in the study area were obtained using the spatial interpolation tool of the ArcGIS-10.8 software [36–38].

Currently, for the disaster susceptibility evaluation unit, division methods include raster, geomorphological, geographical, administrative, and slope division [39,40]. The raster unit can be quickly divided into regional units. However, conducive to the computer's analysis and superposition of the operation, in this study, we adopted the grid unit for the division and conducted re-sampling to 30 m × 30 m evaluation units, with a total of 47,604 rasters. Data sources are shown in Table 1.

Table 1. Data collection.

Datasets	Timeframe	Data Sources	Note
Disaster point data	2023–2024	Field surveys in conjunction with drones	Resolution: 12.5 m
DEM	2023	Geospatial data cloud download (we accessed it on 5 October 2020. https://www.gscloud.cn/)	
Meteorological data	2023–2024	Meteorological station	

3. Methodology

The deterministic coefficient model can quickly analyze the weight of each factor, but there is a sensitivity of each factor to the evaluation of susceptibility, whereas the geo-probe detects the relationship between the influencing factors and the geographic phenomena without any linear assumptions, and gives a weighting coefficient for each factor that depends on its importance for avalanche occurrence, which can bypass the influence of subjective factors on the evaluation results. By coupling probes, the shortcomings of a single CF model can be compensated for.

3.1. Certainty Factor

The CF method is a probability function [32] that has been commonly used in probabilistic analysis to analyze the credibility factors of factors that influence the occurrence of an event. The CF index is computed as follows:

$$CF = \begin{cases} \frac{PP_a - pp_s}{PP_s(1-pp_a)} \ (PP_a < pp_s) \\ \frac{PP_a - pp_s}{PP_a(1-pp_s)} \ (PP_a \geq pp_s) \end{cases}, \quad (1)$$

where PP_a is the probability of avalanche hazards occurring in evaluation factor classification a, and PP_s is the a priori probability of avalanche hazards occurring in the entire study area. In practical applications, PP_a can be the ratio of the number of avalanche hazards in evaluation factor classification a to the area occupied by evaluation factor classification a. PP_s is the ratio of the number of avalanche hazards in the study area to the total area of the study area. When the result of the calculation is positive, avalanche disasters easily occur in the unit, and the closer the CF value is to 1, the more likely avalanches are to occur. When the result of the calculation is negative, avalanche disasters do not easily occur in the unit, and the closer the CF value is to -1, the less likely avalanches are to occur.

3.2. Geodetector

The Geodetector (GD) is a statistical model for detecting spatial heterogeneity and revealing drivers of hazards, and it can be used to analyze the relative weights of avalanche impact factors [41]. Geodetectors can detect the relationship between influencing factors and geographic phenomena without any linear assumptions and can bypass the influence of subjective factors on the evaluation results [42,43].

$$SSW = \sum_{h=1}^{L} N_h \sigma_h^2, \ \ SST = N\sigma^2 \quad (2)$$

where h is the classification of the factor, N_h is the number of cells in classification h, and N is the number of cells in the study area. σ_h^2 and σ^2 are the variances of the Y values in stratum h and the entire area, respectively; SSW and SST are the sum of the intra-stratum variance and the total variance in the entire region, respectively; the q-value denotes the contribution of the individual influencing factors; this value is computed as follows:

$$q = 1 - \frac{\sum_{h=1}^{L} N_h \sigma_h^2}{N\sigma^2} = 1 - \frac{SSW}{SST} \quad (3)$$

3.3. Coupling Model

First, 83 avalanche hazard sample points in the transportation corridor were selected, and an equal number of non-avalanche points were randomly selected, resulting in a total of 166 independent attribute samples. Nine avalanche hazard influence factors were comprehensively selected, and the frequency ratio method was used to analyze the factors influencing the avalanche hazard spatial distribution. The CF value under the grading of each factor was calculated using the certainty coefficient, and the sensitivity of each factor to avalanche hazards was calculated using the Geodetector. Finally, the weights calculated using the Geodetector were weighted and analyzed using the CF value. Stacking of CF and CF-GD values was performed through GIS software version 10.8, and the natural breakpoint method was used to divide the avalanche susceptibility in the study area into extremely high susceptibility, high susceptibility, medium susceptibility, and low susceptibility zones. Finally, the ROC curves were used to compare the evaluation accuracies of the two models. The specific evaluation technical route is shown in Figure 3.

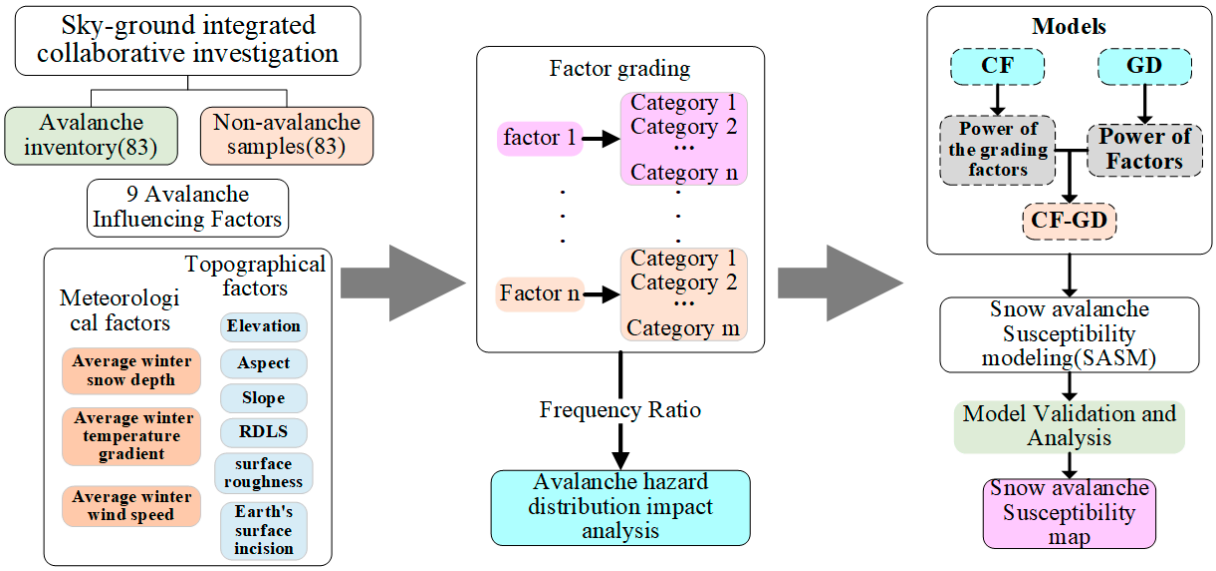

Figure 3. Flowchart of the methodology.

4. Analysis of Factors Affecting the Spatial Distribution of Avalanches

The selection of the influencing factors is the basis for conducting avalanche hazard susceptibility, and topographic data are constant parameters in predicting avalanches. The elevation and slope can reflect the magnitude and frequency of avalanches, and the composite parameters, such as the relief degree of land surface (RDLS), surface incision, and surface roughness, are used to measure the avalanche stability and reveal the relationship between the geomorphology and snow accumulation. The relationship between the landform morphology and snowpack is revealed [11]. Snowfall, wind, and temperature are meteorological factors that trigger avalanches [43,44]. Avalanches caused by heavy snowfall occur more frequently in the Tien Shan mountains, especially in early February when heavy snowfall is frequent [45]. The secondary transport effect of wind causes differences in the distribution of the snow depth across a valley, and changes in wind speed affect the density of the snowpack, thus increasing the instability of the snowpack. Temperature plays a decisive role in the formation of avalanches, and when the temperature gradient is large, deep frost with coarser grains, a brittle structure, and lower cohesion forms, reducing the stability of the snow cover [46]. Nine topographic and climatic influencing factors were selected. The topographic parameters include the slope, slope direction, elevation, topographic relief, ground roughness, and surface cut, while the climatic parameters include the average monthly winter temperature gradient, average winter wind speed, and average winter snow depth.

The frequency ratio (FR) model is a quantitative analysis model that can intuitively reflect the probabilistic relationship between avalanche hazards and impact factors in geospace. For avalanche hazards, the practical application is expressed as categorizing and calculating the affiliation degree of each level of an influence factor to avalanches, which is calculated as follows:

$$FR_{ij} = \frac{A_{ij}/A}{B_{ij}/B} \quad (4)$$

where A is the total number of avalanche hazards in the study area; B is the total area of the study area; A_{ij} is the number of hazards under the grading of each influence factor; and B is the area of the study area under the grading of each influence factor. The oFR_{ij} value reflects the importance of the factors under the grading for the occurrence of an avalanche. $FR_{ij} > 1$ indicates that the influencing factors under the grading are favorable for the occurrence of hazards, and $FR_{ij} < 1$ indicates that the influencing factors under the grading are unfavorable for the occurrence of hazards.

The snow depth is directly related to the triggering of avalanches. By using ArcGIS spatial interpolation tools and weather station data to deduce the winter snow depth in other regions, we determined that the average snow depth in winter in the study area was 32–85 cm, and the slope was reclassified into five levels: 32–40 cm, 40–50 cm, 50–60 cm, 60–70 cm, and 70–85 cm. The average snow depth in most areas of the transportation corridor was around 50–70 cm. When the snow depth exceeds 40 cm, the frequency ratio is 1.01, and the probability of avalanches is higher. The frequency ratio increases with the increase in the snow depth. When the snow depth exceeds 70 cm, the frequency ratio reaches 1.24, and avalanches have the highest probability of occurring under this single condition. When the frequency ratio is 1.01, the probability of avalanches occurring is 1.24. The frequency ratio increases with increasing snow depth. Details are shown in Figure 4.

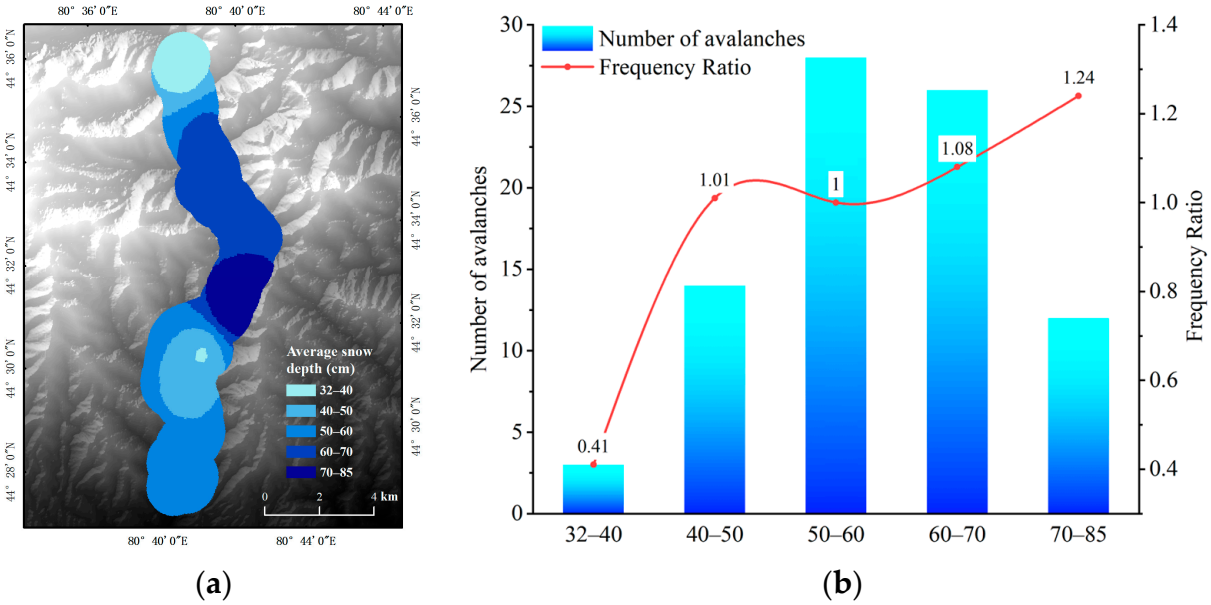

Figure 4. (**a**) Average winter snow depth; (**b**) average winter snow depth frequency ratio.

The wind affects the density and stability of the snow layer, facilitating the triggering of avalanche disasters. The ArcGIS spatial interpolation tool and weather station data were used to derive the average winter wind speeds in other regions. The average winter wind speeds in the study area were around 0.9–2.6 m/s. The average winter wind speeds were reclassified into five levels: 0.9–1.3 m/s, 1.3–1.6 m/s, 1.6–2 m/s, 2–2.3 m/s, and 2.3–2.6 m/s. When the monthly mean wind speed increases to 1.6 m/s, the frequency ratio is 1.06, which favors avalanches. Details are shown in Figure 5.

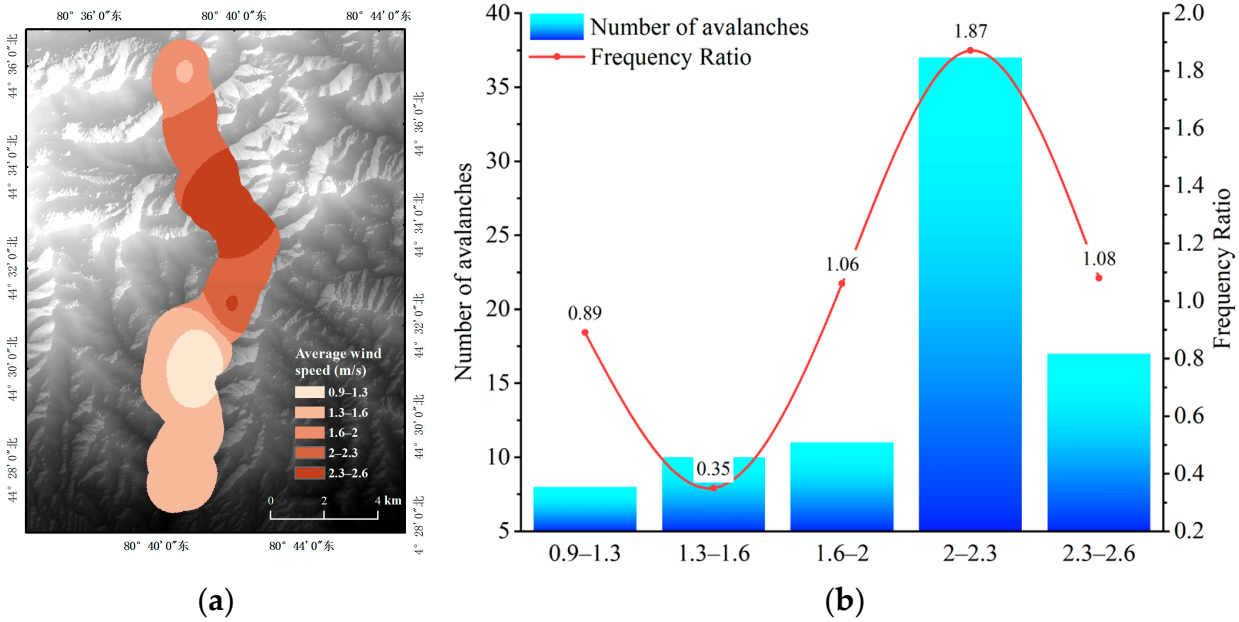

Figure 5. (**a**) Average winter wind speed; (**b**) average winter wind speed frequency ratio.

Temperature plays a decisive role in the formation of avalanches, and the ArcGIS spatial interpolation tool and weather station data were used to derive the gradient of the monthly mean temperature change in winter in other regions. The temperature gradient in the study area was around 9.5–12.5 °C/month, and the temperature gradient was reclassified into five levels: 9.5–10.5 °C, 10.5–11 °C, 11–11.5 °C, 11.5–12 °C, and 12–12.5 °C. As the gradient of the temperature change increases, the frequency ratio tends to increase. When the monthly average temperature change gradient reaches 11 °C/month, the frequency ratio is 1.03, which indicates that the probability of avalanche occurrence in the transportation corridor is higher when the monthly average temperature change gradient exceeds 11 °C/month. When the temperature gradient exceeds 12 °C/month, the frequency ratio reaches a maximum of 1.14, and the probability of avalanche occurrence is the highest under this single condition. Details are shown in Figure 6.

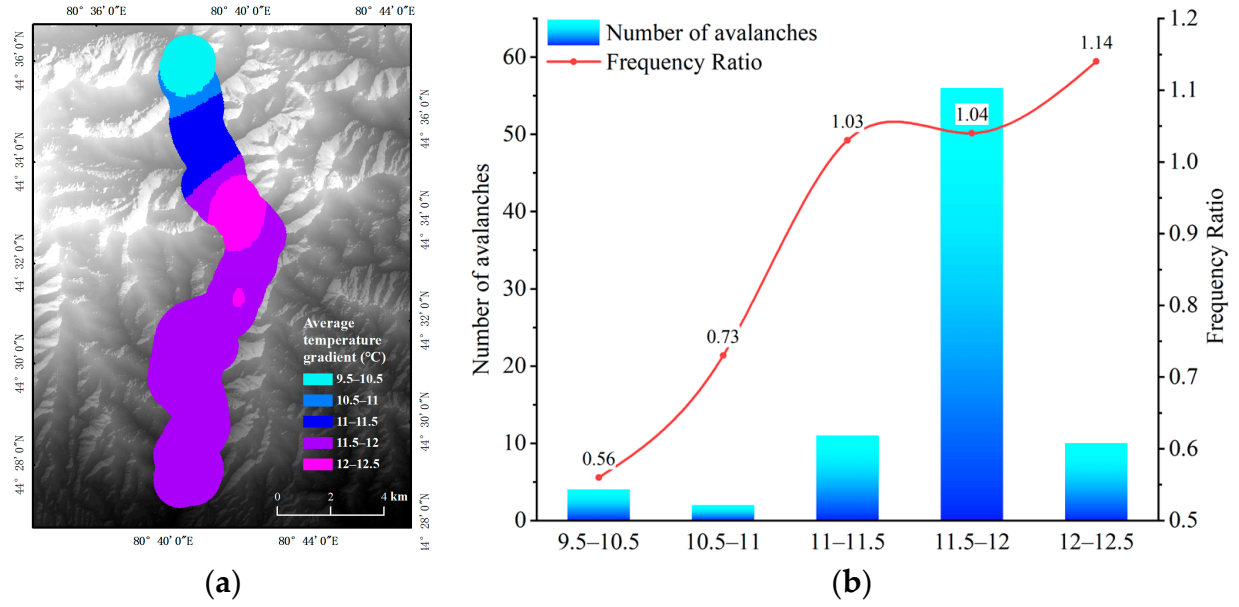

Figure 6. (**a**) Average winter temperature; (**b**) average winter temperature frequency ratio.

The surface roughness is the ratio of the curved surface area of a surface unit to its projected area on the horizontal plane. The surface roughness is a macro-terrain factor that reflects the degree of relief and erosion of the terrain [47]. The DEM surface roughness of the study area with a 12.5 m spatial resolution was calculated by using ArcGIS software, and the surface roughness was reclassified into five levels: 1–1.08, 1.08–1.16, 1.16–1.24, 1.24–1.36, and 1.36–2.6. As the surface roughness increases, the frequency ratio initially increases and then decreases, with surface roughness values of 1.6–1.36. A frequency ratio of >1 is favorable for avalanche-prone area development. For surface roughness values of 1.24–1.36, the maximum frequency value is 1.54, and the probability of avalanches occurring under this single condition is the largest. Details are shown in Figure 7.

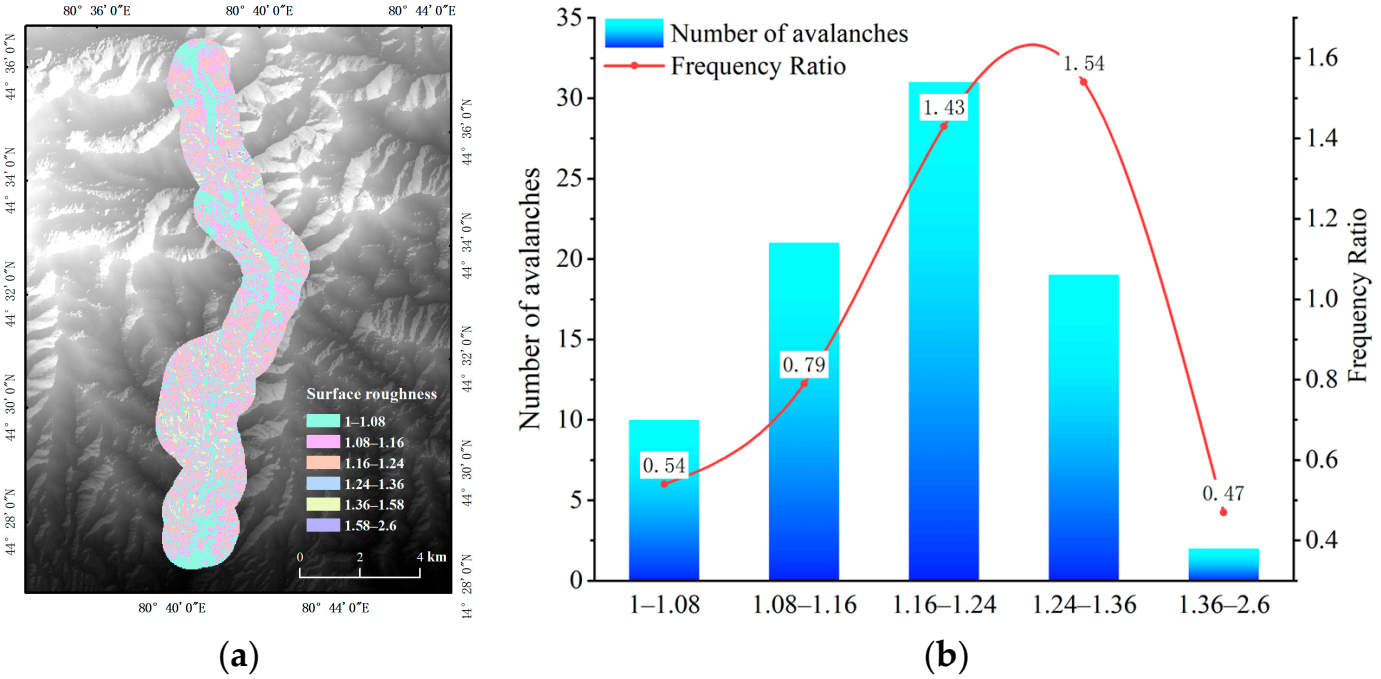

Figure 7. (**a**) Surface roughness; (**b**) surface roughness frequency ratio.

The relief degree of a land surface refers to the height difference between the highest point and the lowest point in a specific area, and it can directly reflect the regional relief characteristics [48]. It is a quantitative index that describes the regional geomorphology, and it is also an important indicator for natural disaster assessment. The DEM relief degree of the land surface with a 12.5 m spatial resolution for the study area was calculated using ArcGIS software, and the relief degree of the land surface was reclassified into five levels: 0–100, 100–200, 200–300, 300–400, and 400–500. As the relief degree of the land surface increases, the frequency ratio initially increases and then decreases, and the relief degree of the land surface is within the range of 300–500, with a frequency ratio of >1, which is favorable for avalanche occurrence under this condition. Details are shown in Figure 8.

The surface incision refers to the difference between the average elevation and the lowest elevation within the area adjacent to a point, which can reflect the condition of erosion cutting into the surface [49]. The DEM of the surface incision with a 12.5 m spatial resolution for the study area was calculated using ArcGIS software, and the surface incision was reclassified into five classes: 0–50, 50–100, 100–150, 150–200, and 200–250. As the surface incision increases, the frequency ratio tends to increase and then decrease, and within the surface incision range of 100–200, the frequency ratio is >1, making avalanches more likely to occur under this condition. Details are shown in Figure 9.

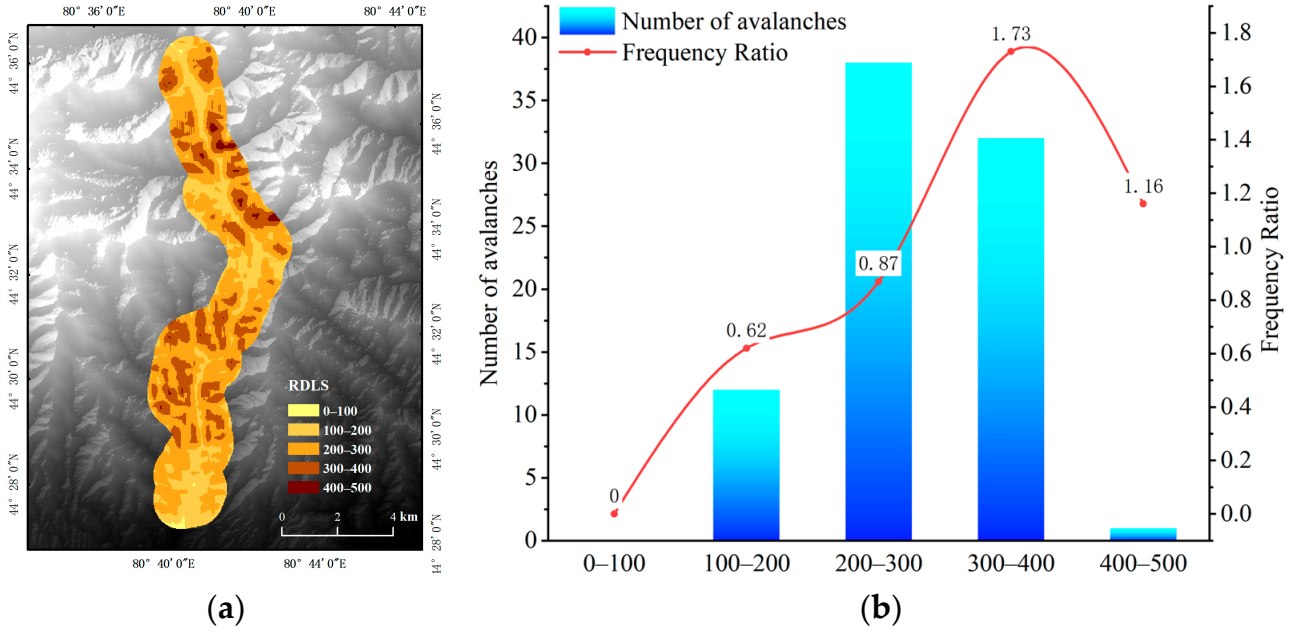

Figure 8. (**a**) Relief degree of land surface; (**b**) relief degree of land surface frequency ratio.

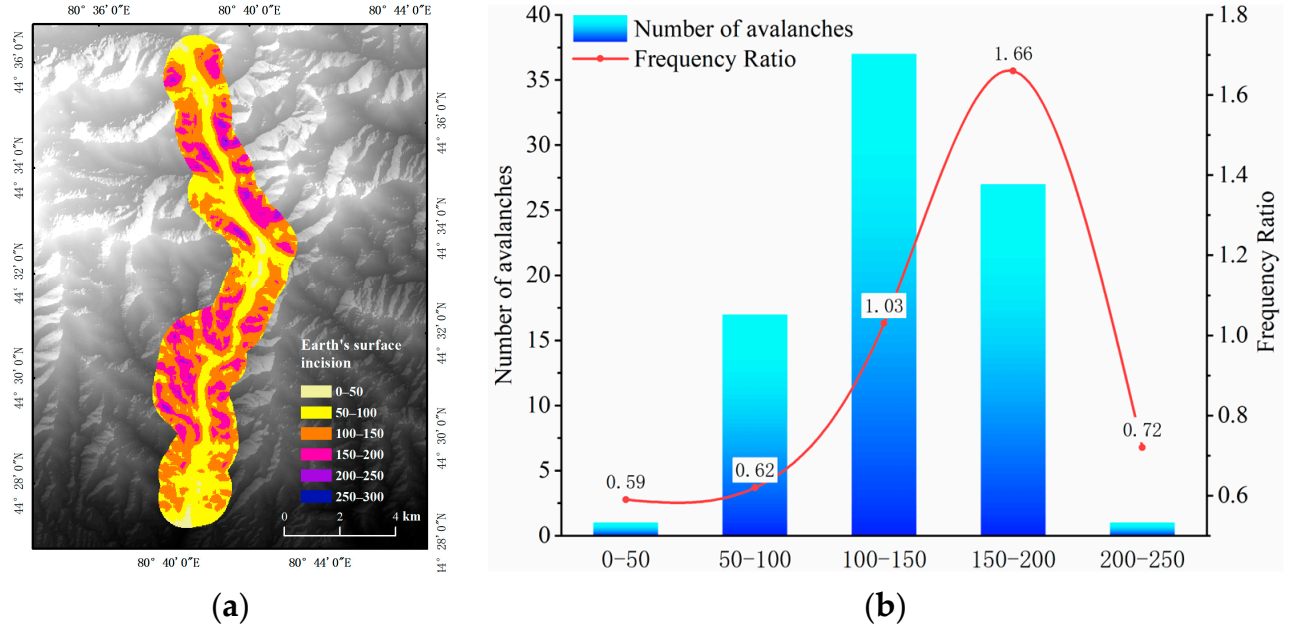

Figure 9. (**a**) Surface incision; (**b**) surface incision frequency ratio.

Avalanches are sensitive to slopes, and a slope that is too low or too high is detrimental to the development of avalanche hazards. The DEM of the slope with a 12.5 m spatial resolution for the study area was calculated using ArcGIS software, and the slope was reclassified into six levels: 0–10°, 10–20°, 20–30°, 30–40°, 40–50°, and >50°. Traffic corridor areas mainly have slopes of 20–40°, and they are concentrated between 30° and 40°. As the slope increases, the frequency ratio gradually increases. The maximum value of the frequency ratio occurs in areas with slopes of 30–40°, and the frequency ratio decreases when the slope is >40°, indicating that the slopes most favorable for avalanche development are 30–40°, <20°, and >50°. The frequency ratio of <20° and >50° slopes is <1, which is not favorable for avalanche development. Details are shown in Figure 10.

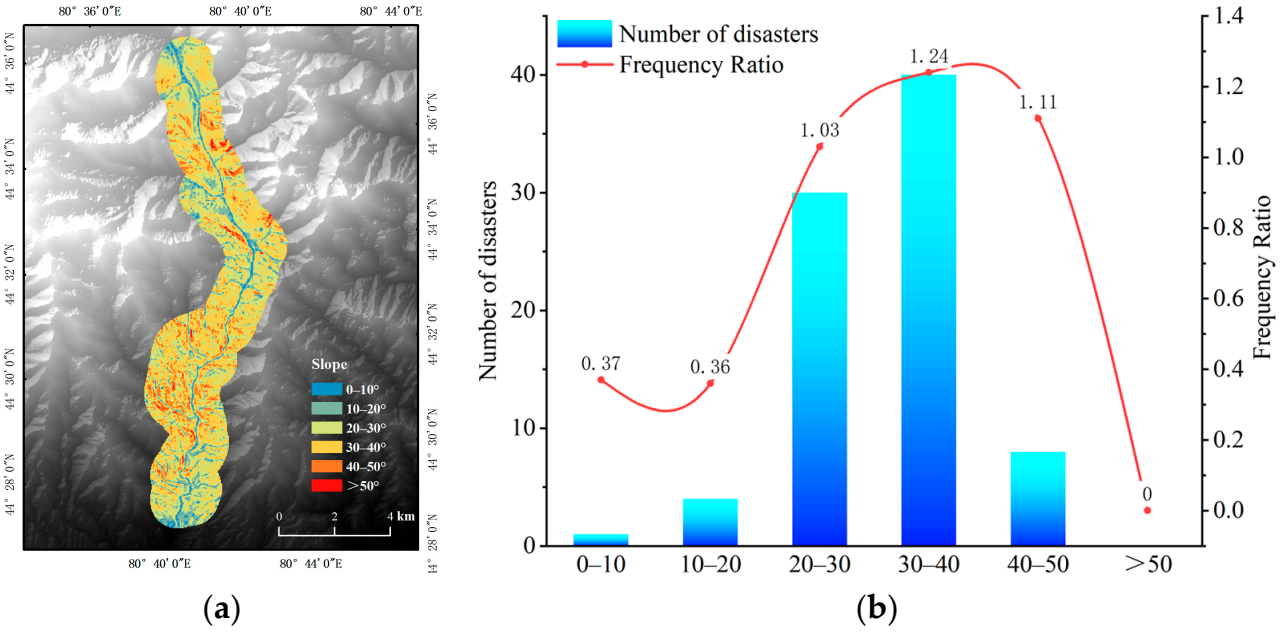

Figure 10. (**a**) Slope; (**b**) frequency ratio.

As the sunshine, snowfall, and wind speed are different for different slope aspects, the snow depth and snow layer characteristics are different for different slope aspects, which further affects avalanche development. The DEM of the slope aspect of the study area with a 12.5 m spatial resolution was calculated using ArcGIS software, and the slope aspect was reclassified into eight classes ((19)): north (337.5–22.5°), northeast (22.5–67.5°), east (67.5–112.5°), southeast (112.5–157.5°), south (157.5–202.5°), southwest (202.5–247.5°), west (247.5–292.5°), and northwest (292.5–337.5°). The calculation results show that the east, southeast, and northwest slope aspects are favorable for the development of avalanche hazards in the transportation corridor. The frequency ratios are all >1, and the largest frequency ratios are for the east and northwest slope aspects. Details are shown in Figure 11.

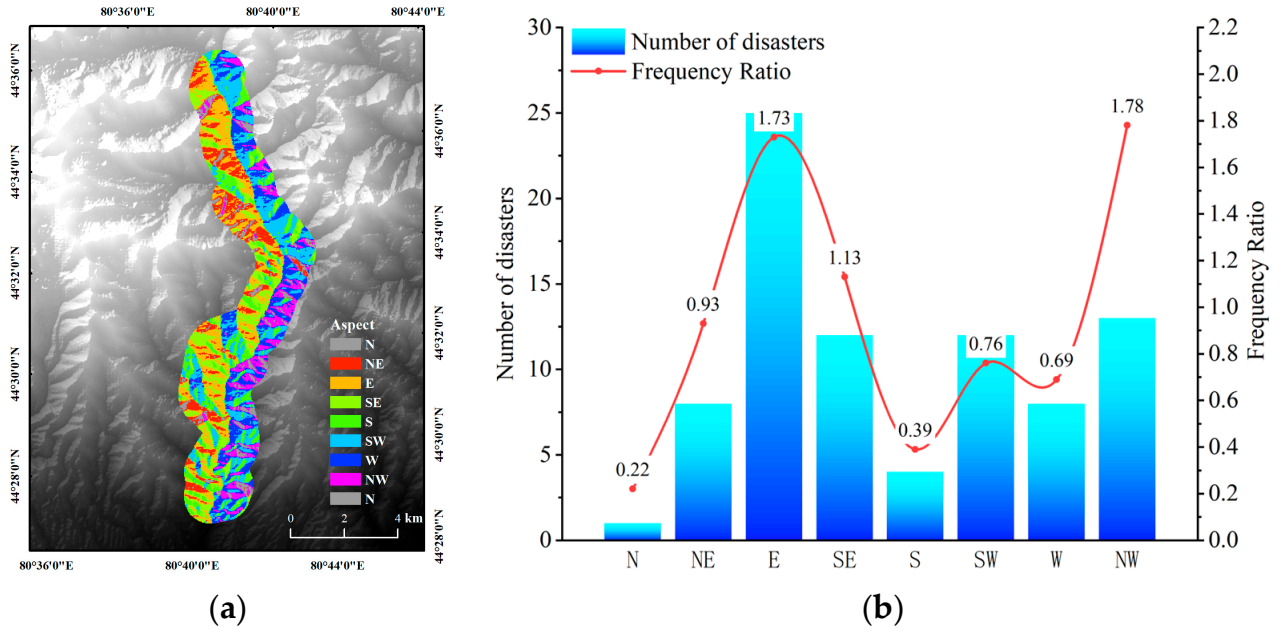

Figure 11. (**a**) Aspect; (**b**) aspect frequency ratio.

Elevation is one of the factors influencing the occurrence of avalanche disasters. The DEM of the elevation with a 12.5 m spatial resolution was extracted using ArcGIS software. The elevation in the study area ranged from 1422 to 3497 m, and the elevation was reclassified into five levels ((21)): 1–1.5 km, 1.5–2 km, 2–2.5 km, 2.5–3 km, and 3–3.5 km. In the transportation corridor, the elevations were mainly between 1.5 and 3 km. As the elevation increases, the frequency ratio increases and then decreases. The maximum frequency ratio is 1.79 when the elevation is in the range 2–2.5 km, which indicates that elevations of 2–2.5 km in the study area are the most favorable for the occurrence of avalanche disasters. Details are shown in Figure 12.

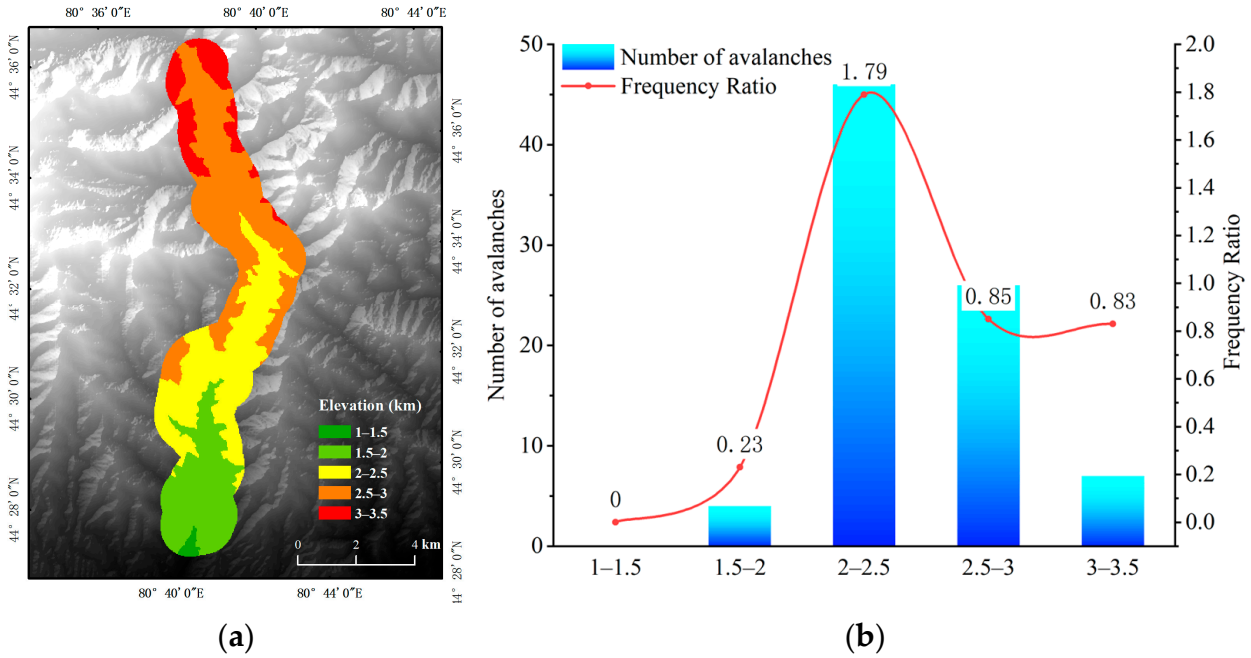

Figure 12. (**a**) Elevation; (**b**) elevation frequency ratio.

5. Results

5.1. Selection of Avalanche-Influencing Factors

The frequency ratios of nine influence factors, namely, meteorological factors (mean winter temperature gradient, mean winter snow depth, and mean winter wind speed) and topographic factors (elevation, aspect, slope, relief degree of land surface, ground roughness, and surface incision), were obtained via calculations (Table 2). The results show that all nine factors played a positive role in avalanche development. Thus, our vulnerability evaluation is based on these nine factors. The calculation results of the evaluation factors are shown in Table 2.

Table 2. Evaluation factor frequency ratios, CF, and GD.

Factors	Factor Grading	Frequency Ratio	CF	GD
Average temperature gradient	9.5–10.5	0.56	−0.44	0.35
	10.5–11	0.73	−0.27	
	11–11.5	1.04	0.03	
	11.5–12	1.04	0.04	
	12–12.5	1.14	0.12	
Average snow depth	32–40	0.41	−0.59	0.25
	40–50	1.01	0.01	
	50–60	1.00	0.00	
	60–70	1.08	0.07	
	70–85	1.24	0.19	

Table 2. *Cont.*

Factors	Factor Grading	Frequency Ratio	CF	GD
Average wind speed	0.9–1.3	0.89	−0.11	0.17
	1.3–1.6	0.35	−0.65	
	1.6–2	1.07	0.06	
	2–2.3	1.87	0.47	
	2.3–2.6	1.08	0.07	
Surface roughness	1–1.08	0.54	−0.46	0.13
	1.08–1.16	0.80	−0.20	
	1.16–1.24	1.43	0.30	
	1.24–1.36	1.54	0.35	
	1.36–2.6	0.47	−0.53	
Surface incision	0–50	0.59	−0.41	0.11
	50–100	0.62	−0.38	
	100–150	1.03	0.03	
	150–200	1.66	0.40	
	200–250	0.72	−0.28	
RDLS	0–100	0.00	0.00	0.12
	100–200	0.62	−0.38	
	200–300	0.87	−0.13	
	300–400	1.73	0.42	
	400–500	1.16	0.13	
Elevation	1–1.5 km	0.00	0.00	0.15
	1.5–2 km	0.23	−0.77	
	2–2.5 km	1.79	0.44	
	2..5–3 km	0.85	−0.15	
	3–3.5 km	0.83	−0.17	
Aspect	N	0.22	−0.78	0.75
	NE	0.94	−0.06	
	E	1.73	0.42	
	SE	1.13	0.12	
	S	0.39	−0.61	
	SW	0.76	−0.24	
	W	0.69	−0.31	
	NW	1.77	0.44	
Slope	0–10°	0.37	−0.63	0.55
	10–20°	0.36	−0.64	
	20–30°	1.03	0.03	
	30–40°	1.24	0.19	
	40–50°	1.11	0.10	
	>50°	0.00	0.00	

5.2. CF Model Results

The value of the coefficient of determination (CF) for each of the nine evaluation factors was calculated using Equation (1). The calculation results are presented in Table 2. The avalanche susceptibility of the traffic corridors was classified by ArcGIS-10.8 software, where the calculated CF values were first superimposed and reclassified into four classes by the natural breaks (Jenks) method: very high susceptibility, high susceptibility, medium susceptibility, and low susceptibility areas. These susceptibility grades accounted for 14.51%, 25.89%, 32.73%, and 26.87%, respectively. The zoning results are shown in Table 3. Among them, the extremely high susceptibility zone and high susceptibility zone accounted for 59.6%, and they were located on both sides of the river valley in the middle and upper parts of the transportation corridor. The results of the calculations are shown in Table 3.

Table 3. Comparison of different model predictions.

Susceptibility Level	CF				GD-CF			
	Area (km^2)	Area Ratio	Avalanche Number	Avalanche Ratio	Area (km^2)	Area Ratio	Avalanche Number	Avalanche Ratio
Low	6.04	14.51%	2.00	2.41%	4.75	11.40%	3.00	3.61%
Medium	10.79	25.89%	4.00	4.82%	11.91	28.60%	5.00	6.02%
High	13.64	32.73%	23.00	27.71%	15.52	37.27%	31.00	37.35%
Very high	11.19	26.87%	54.00	65.06%	9.47	22.74%	44.00	53.01%

5.3. Results of the Coupled CF-GD Model

Based on the ArcGIS statistics for the grading of each influencing factor, the relative weights of the avalanche-influencing factors in the transportation corridor were calculated according to the geodetic detector model (Equation (2)), and the results of the analysis and calculation revealed that the contributions of the nine influencing factors to avalanche development, in descending order, were as follows: slope aspect (29.07%), slope angle (21.32%), temperature gradient (13.57%), average snow depth (9.69%), average wind speed (6.59%), elevation (5.81%), surface roughness (5.04%), relief degree of land surface (4.65%), and Surface incision (4.26%). The slope aspect, slope angle, and mean winter temperature gradient contributed a proportion of 63.95% to avalanche development, suggesting that topographic and temperature variations have greater influences on avalanche development within transportation corridors. The evaluation factor contributions are shown in Figure 13.

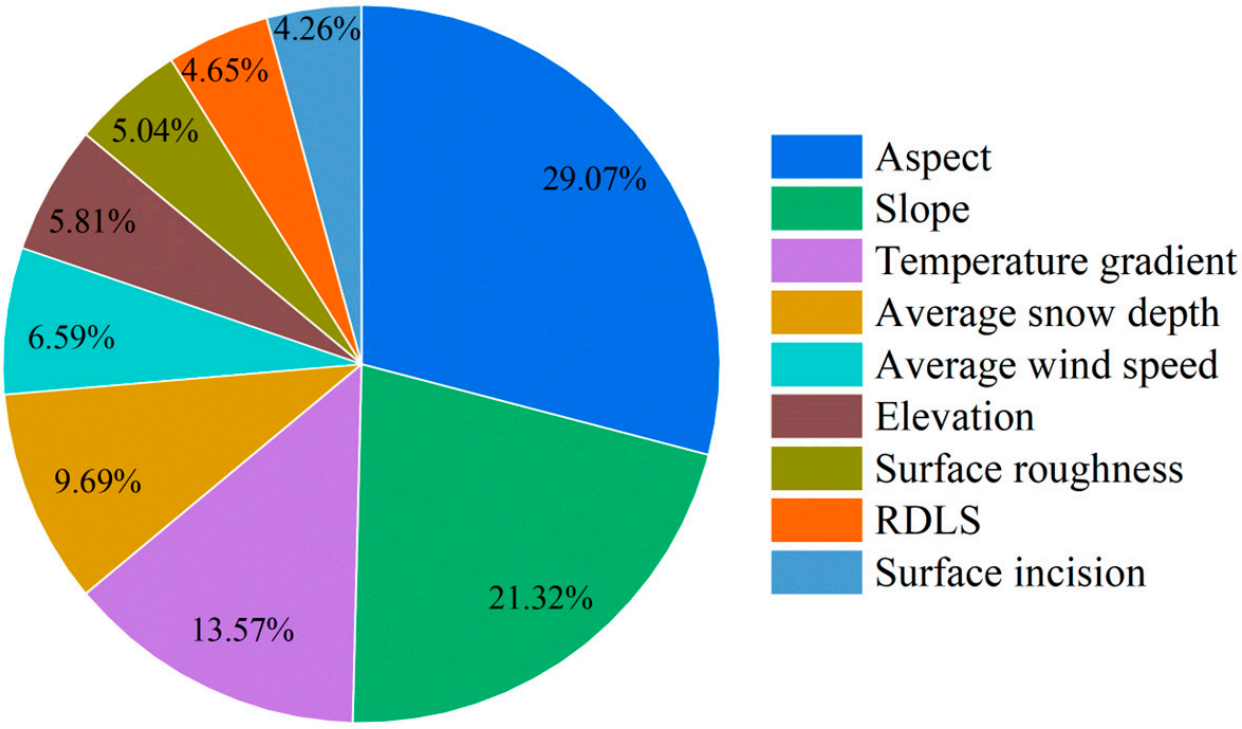

Figure 13. Factor contribution chart.

Using Equations (1) and (2), the affiliation values of the nine avalanche-influencing factors for the transportation corridor were calculated and weighted with the weight values calculated using the geodetic detector to obtain an avalanche susceptibility distribution map for the coupled CF-GD model in the transportation corridor. The traffic corridor susceptibility was classified by ArcGIS-10.8 software, where the calculated CF-GD values were first superimposed and then reclassified into four classes by the natural breaks (Jenks) method. These susceptibility levels accounted for 11.4%, 28.6%, 37.27%, and 22.74%,

respectively, of the study area. The extremely high susceptibility and high susceptibility areas were mainly located on both sides of the valley in the middle part of the transportation corridor. The results are shown in Figure 14b.

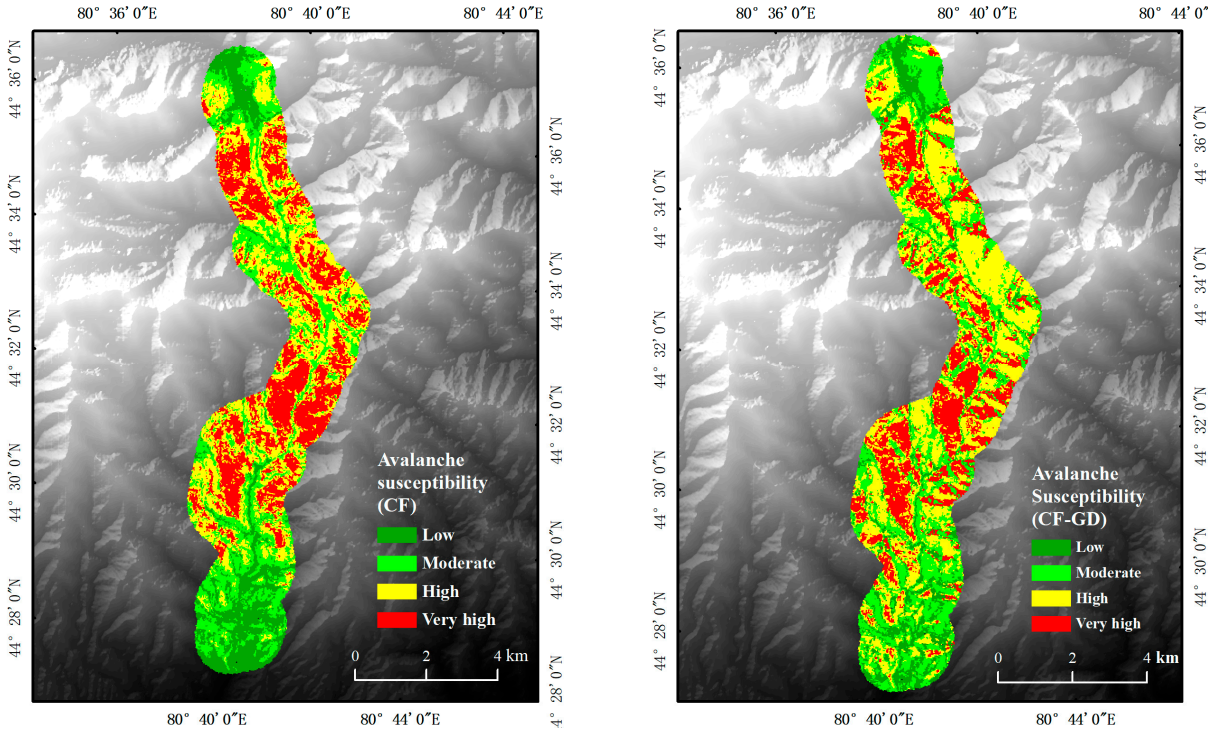

Figure 14. (**a**) Avalanche susceptibility zoning based on CF modeling; (**b**) avalanche susceptibility zoning based on a coupled CF-GD model.

5.4. Validation of Model Results

The two avalanche susceptibility models yielded the same avalanche hazard distribution patterns, i.e., mainly located on both sides of the river valley in the middle section of the transportation corridor. Five large avalanches (1–5) and one potential avalanche point (6) were identified during the site investigation. The highway passes through the flow area or accumulation area of avalanches 1, 2, and 6, and avalanches 3, 4, and 5 will affect the construction. Based on the results of the susceptibility evaluation, the five avalanche points and one potential avalanche point all appear in the very high susceptibility area on the susceptibility map, demonstrating that the results of the evaluation are consistent with the actual situation. The results of the field survey are shown in Figure 15 (1–6#) ('#' is the number of avalanches).

ROC curves are often used for accuracy validation of the susceptibility evaluation model, and the accuracy is expressed as the AUC. A large AUC indicates that the accuracy of the model is higher and the model is more predictive [50]. The percentage accumulation of the susceptible area under the classification represents the horizontal axis specificity, and the percentage accumulation of the avalanche hazard points represents the vertical axis sensitivity [20]. The calculation results are shown in Figure 16. The AUC value of the CF-GD coupling model is 0.889, the AUC value of the deterministic coefficient model is 0.836, and the AUC values of the two models derived from the calculation results are >0.8, so it can be concluded that the model results have a high accuracy, and the CF-GD coupling model has a higher accuracy than the CF model.

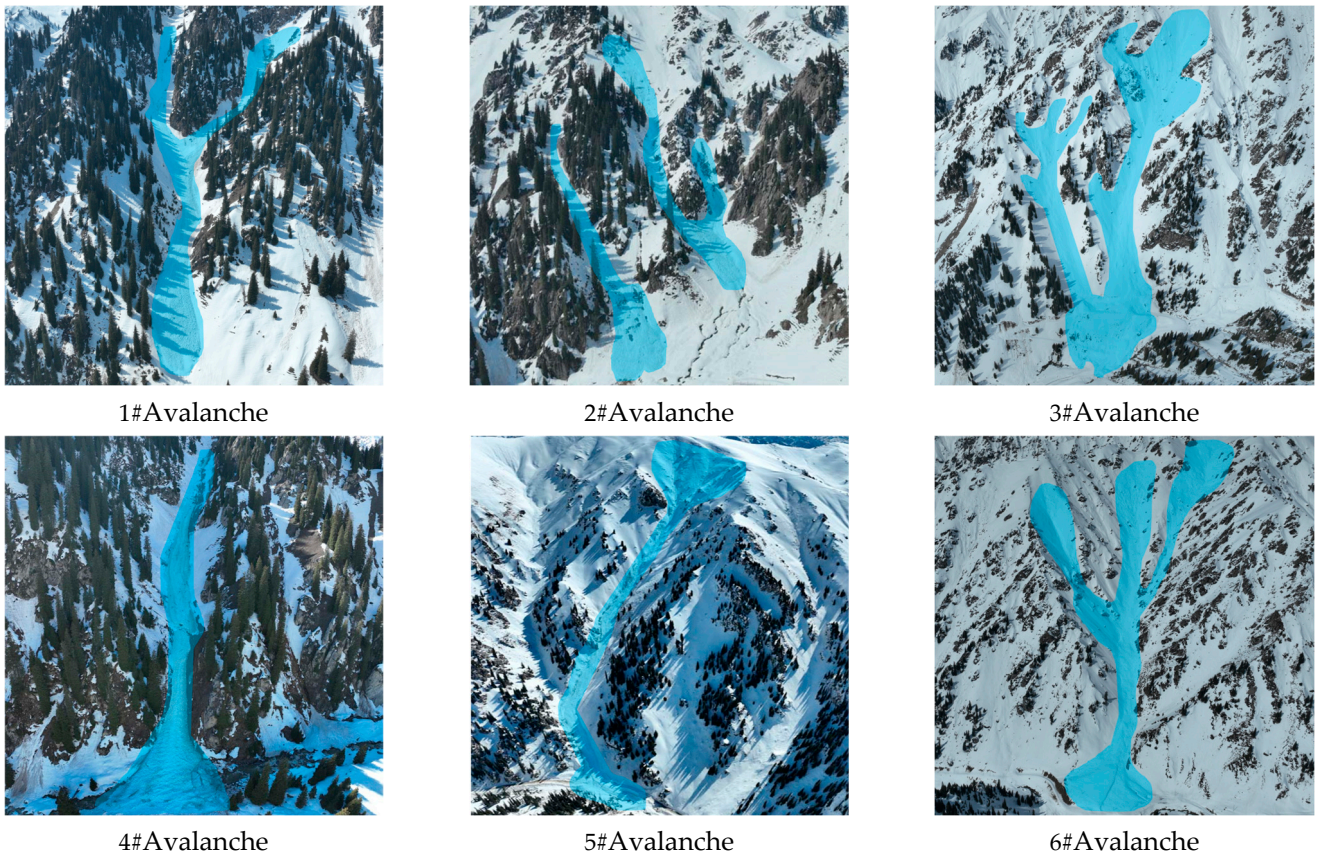

Figure 15. Typical avalanche map of transportation corridors.

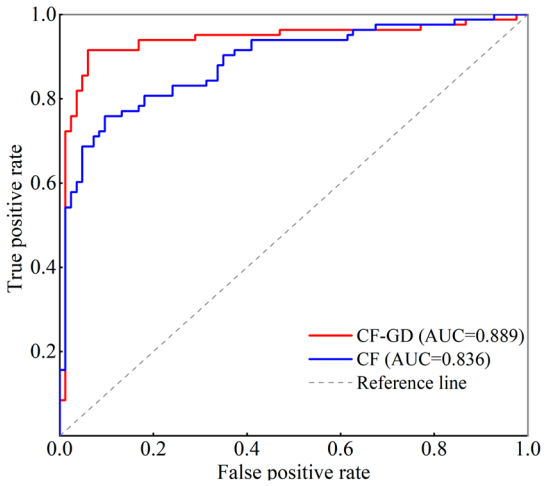

Figure 16. ROC curve analysis.

6. Discussion

Qualitative analysis and quantitative analysis are the mainstream types of avalanche hazard susceptibility evaluation methods at present. Reducing the influence of subjective factors on susceptibility evaluation is the advantage of quantitative analysis methods such as Geodetectors, compared with expert scoring methods such as qualitative analysis methods. The CF model and GD model results intuitively reflect the contributions of the different grading factors to avalanche hazard development and the main controlling factors of avalanche hazard development. The coupled CF-GD model compensates for the fact that the explanatory power of a single model cannot distinguish the influencing factors, and the evaluation accuracy of the coupled model is higher than that of a single model.

This coupling method has higher requirements for the completeness of avalanche sample data, and at this stage, the evaluation is carried out in small-scale regions, and the evaluation accuracy is affected by the quality of avalanche sample data, which cannot fully respond to the relationship between the formation of hazards and the evaluation factors. Under these conditions, this approach could also be applied to areas other than traffic corridors but would need to be tested for applicability. With the development of machine learning, the coupling method combining machine learning and traditional statistical methods will further improve the accuracy of avalanche susceptibility assessment, which requires more avalanche samples to support.

The factor weights calculated using the coupled model revealed that the weight values of the slope aspect and slope angle were the largest, indicating that these two factors played dominant roles in the distribution of the avalanche hazards. The avalanche occurrence is highly sensitive to the slope angle. A slope that is either too steep or too gentle is detrimental to avalanche development, and the effects of solar radiation and wind speed on the snowpack on slopes with different aspects affect the distribution of avalanches. In the future, we will consider using sub-aspects in the susceptibility evaluation to include the mechanism factors affecting avalanche development, such as solar radiation and ground temperature changes, in the evaluation system in order to further analyze the nonlinear relationships between avalanche hazards and different evaluation factors and to improve the evaluation progress.

Most of the highway routes are located in very high and high avalanche susceptibility areas, which seriously threatens infrastructure such as roadbeds, bridge abutments, and tunnel openings. Therefore, these areas require intensified hazard assessment and prevention measures, such as the installation of snow stabilization fences in avalanche initiation zones and the construction of snow guide bunds to alter avalanche flow paths.

7. Conclusions

In order to ensure the smooth flow of transport corridors, and help the economic development and security of the property of mountain people, it is important to carry out avalanche susceptibility assessment in transport corridors. This study identified meteorological and topographical conditions favorable to avalanche occurrence in the transport corridor; the main factors favoring avalanche occurrence in the study area were slope direction, slope angle, and average winter temperature gradient, and a map of avalanche susceptibility in the transport corridor was produced.

The avalanche hazard dataset for the Wen Quan to Khorgos section of the G219Wen Quan to Khorgos transportation corridor was collected through a joint air–ground survey, and nine factors, namely, the mean winter temperature gradient, mean winter snow depth, mean winter wind speed, surface roughness, surface incision, relief degree of the land surface, elevation, slope angle, and slope aspect, were selected to analyze the spatial distribution pattern of avalanche hazards in the transportation corridor. An evaluation system of avalanche disaster susceptibility was further established, and the evaluation accuracies of the coupled CF-GD model and CF model were compared and analyzed. The conclusions that follow were obtained.

(1) The analysis of the influencing factors through the frequency ratio method revealed that among the factors affecting the spatial distribution of avalanche hazards in the transportation corridor from G219Wen Quan to Khorgos, the most favorable ranges for the occurrence of hazards were as follows: snow depth of >40 cm, wind speed of >1.6 m/s, temperature gradient of more than 11 °C, elevations of 2–2.5 km, slope angles of 30–40°, east, southeast, and northwest slope aspects, a surface roughness of >1.16, a relief degree of land surface of >300 m, and a surface incision of >100 m. The main factors favoring avalanche development in the study area were the slope aspect, slope angle, and average winter temperature gradient.

(2) Based on the susceptibility evaluation conducted using the coupled CF-GD model, the study area was divided into four levels: low susceptibility, medium susceptibility,

high susceptibility, and very high susceptibility areas, which accounted for 11.4%, 28.6%, 37.27%, and 22.74% of the total area of the study area, respectively. The high susceptibility area accounted for the largest proportion of the study area, and the low susceptibility area accounted for the smallest proportion of the study area. The very high susceptibility and high susceptibility areas were located in the middle section of the river valley in the middle part of the transportation corridor. The extremely high susceptibility and high susceptibility areas were mainly located in the middle of the valley of the transportation corridor. This is consistent with the results of the field investigation. The results of this study provide support for local avalanche mitigation and prevention.

(3) The accuracy of the evaluation model was verified according to the AUC value. The AUC value of the CF model was 0.836, and the AUC value of the coupled CF-GD model was 0.889. The coupled model had a higher accuracy than the single model, and the accuracy of the coupled model was about 6.34% better compared with the single model. The coupled model is more suitable for avalanche susceptibility evaluation; coupled models are more accurate than single-model avalanche susceptibility zoning maps and can provide more precise information for avalanche control. Our research method can be used as a reference for other avalanche-prone mountain areas.

(4) The coupled CF-GD model can generate a reliable snow avalanche susceptibility mapping that has a sound scientific basis for preventing and mitigating damage caused by avalanches. Therefore, the methods outlined in this paper should be tested through application in other areas as they may improve avalanche susceptibility assessments in other avalanche-prone areas.

Author Contributions: Conceptualization, J.L., X.S., Z.Y. and C.H.; methodology, J.L., X.S., Z.Y. and B.W.; software, X.S. and S.Y; validation, X.S. and S.Y.; formal analysis, X.S. and S.Y.; investigation, J.L., X.S., C.H., B.W., Z.Y., Q.G., S.Y. and H.X.; resources, J.L. and C.H.; data curation, X.S., S.Y. and C.H.; writing—original draft preparation, J.L. and X.S.; writing—review and editing, J.L. and X.S.; visualization, Z.Y.; supervision, C.H.; project administration, Z.Y., Q.G. and B.W.; funding acquisition, J.L. and C.H. All authors have read and agreed to the published version of the manuscript.

Funding: This research was funded by the key Science and Technology projects in the transportation industry, grant number 2022-ZD6-090; the Xinjiang Transportation Science and Technology Project, grant number 2022-ZD-006; the Xinjiang Jiaotou Group's 2021 annual "unveiling of the list of commanders" science and technology project, grant number ZKXFWCG2022060004; and the Xinjiang Transportation Design Institute Science and Technology R&D Project, grant number KY2022021501.

Institutional Review Board Statement: Not applicable.

Informed Consent Statement: Not applicable.

Data Availability Statement: Data is contained within the article. The original contributions presented in the study are included in the article, further inquiries can be directed to the corresponding author.

Conflicts of Interest: Jie Liu, Xiliang Sun, Zhiwei Yang, Bin Wang, Senmu Yao and Changtao Hu are employees of Xinjiang Transport Planning Survey and Design Institute Co., Ltd. The paper reflects the views of the scientists and not the company.

References

1. Qin, D.; Yao, T.; Ding, Y.; Ren, J. Establishment and significance of the cryosphere scientific system. *Bull. Chin. Acad. Sci.* **2020**, *35*, 14.
2. Wang, S.; Yang, Y.; Che, Y.; Che, Y. Global Snow- and Ice-Related Disaster Risk: A Review. *Nat. Hazards Rev.* **2022**, *23*, 03122002. [CrossRef]
3. Wang, S.; Wen, J. Characteristics, Influence of Cryosphere Disaster and Prospect of Discipline Development. *Bull. Chin. Acad. Sci.* **2020**, *35*, 8.
4. Wang, P.; Li, H.; Li, Z.; Yu, F.; He, J.; Dai, Y.; Wang, F.; Chen, P. Cryosphere changes and their impacts on regional water resources in the Chinese Altai Mountains from 2000 to 2021. *Catena* **2024**, *235*, 107644. [CrossRef]

5. Durlević, U.; Valjarević, A.; Novković, I.; Ćurčić, N.; Smiljić, M.; Morar, C.; Stoica, A.; Barišić, D.; Lukić, T. GIS-Based Spatial Modeling of Snow Avalanches Using Analytic Hierarchy Process. A Case Study of the Šar Mountains, Serbia. *Atmosphere* **2022**, *13*, 1229. [CrossRef]
6. Hao, J.; Li, L. Progress and prospect of avalanche disaster prevention and control research. *Glaciol. Geocryol.* **2022**, *44*, 762–770. [CrossRef]
7. Thangavelu, A.; Sridhar, R.; Sapna, K.; Velusamy, S.; Shanmugamoorthy, M.; Shanmugavadivel, S. Bayesian networks and intelligence technology applied to climate change: An application of fuzzy logic based simulation in avalanche simulation risk assessment using GIS in a Western Himalayan region. *Urban Clim.* **2022**, *45*, 101272, ISSN 2212-0955. [CrossRef]
8. Qin, Q.; Li, X.; Hao, J.; Zhang, B.; Li, Q.; Gong, Z. Zoning of avalanche hazard and its spatial and temporal patterns in the Tianshan Mountains of China. *Nat. Disasters* **2023**, *32*, 117–124. [CrossRef]
9. Yang, J.; Zhang, X.; Mao, W.; He, Q. Investigation and analysis of snow avalanche disaster Tianshan Mountains of China. *J. Nat. Disasters* **2022**, *31*, 188–197. [CrossRef]
10. Rahmati, O.; Ghorbanzadeh, O.; Teimurian, T.; Mohammadi, F.; Tiefenbacher, J.P.; Falah, F.; Pirasteh, S.; Ngo, P.-T.T.; Bui, D.T. Spatial modeling of snow avalanche using machine learning models and Geo-Environmental factors: Comparison of effectiveness in two mountain regions. *Remote Sens.* **2019**, *11*, 2995. [CrossRef]
11. Liu, J.; Zhang, T.; Hu, C.; Wang, B.; Yang, Z.; Sun, X.; Yao, S. A Study on Avalanche-Triggering Factors and Activity Characteristics in Aerxiangou, West Tianshan Mountains, China. *Atmosphere* **2023**, *14*, 1439. [CrossRef]
12. Liapidevskii, V.Y.; Dutykh, D. On the velocity of turbidity currents over moderate slopes. *Fluid Dyn. Res.* **2019**, *51*, 035501. [CrossRef]
13. Liapidevskii, V.Y.; Dutykh, D.; Gisclon, M. On the modelling of shallow turbidity flows. *Adv. Water Resour.* **2018**, *113*, 310–327. [CrossRef]
14. Dutykh, D.; Acary-Robert, C.; Bresch, D. Mathematical Modeling of Powder-Snow Avalanche Flows. *Stud. Appl. Math.* **2011**, *127*, 38–66. [CrossRef]
15. Ivanova, K.; Caviezel, A.; Buhler, Y.; Bartelt, P. Numerical modelling of turbulent geophysical flows using a hyperbolic shear shallow water model: Application to powder snow avalanches. *Comput. Fluids* **2022**, *233*, 105211. [CrossRef]
16. Yang, T. Research on the avalanche disaster monitoring and warning technology in southline of Sichuan-Tibet highway in territory Tibet. *China Sci.* **2018**, *13*, 921–925.
17. Arnous, M.O.; Aboulela, H.A.; Green, D.R. Geo-environmental hazards assessment of the north western Gulf of Suez, Egypt. *J. Coast. Conserv.* **2011**, *15*, 37–50. [CrossRef]
18. Valjarević, A. GIS-Based Methods for Identifying River Networks Types and Changing River Basins. *Water Resour. Manag.* **2024**, 1–19. [CrossRef]
19. Bahram, C.; Moslem, B.; Amir, M.; Sajedi-Hosseini, F.; Shamshirban. Snow avalanche hazard prediction using machine learning methods. *J. Hydrol.* **2019**, *577*, 123929, ISSN 0022-1694. [CrossRef]
20. Yang, D.; Zhu, J.; Liu, S.; Ma, B.; Dai, X.S. Comparative analyses of susceptibility assessment for landslide disasters based on information value, weighted information value and logistic regression coupled model in Luoping County, Yunnan Province. *Chin. J. Geol. Hazard Control* **2023**, *34*, 43–53. [CrossRef]
21. Yariyan, P.; Omidvar, E.; Minaei, F.; Ali Abbaspour, R.; Tiefenbacher, J.P. An optimization on machine learning algorithms for mapping snow avalanche susceptibility. *Nat. Hazard* **2022**, *111*, 1–36. [CrossRef]
22. Durlević, U.; Novković, I.; Bajić, S.; Milinčić, M.; Valjarević, A.; Čegar, N.; Lukić, T. Snow Avalanche Hazard Prediction Using the Best-Worst Method—Case Study: The Šar Mountains, Serbia. In *The International Workshop on Best-Worst Method*; Springer Nature Switzerland: Cham, Switzerland, 2023; pp. 211–226. [CrossRef]
23. Liu, Y.; Chen, X.; Yang, J.; Wang, T. Snow avalanche susceptibility mapping from tree-based machine learning approaches in ungauged or poorly-gauged regions. *Catena* **2023**, *224*, 106997. [CrossRef]
24. Fromm, R.; Schönberger, C. Estimating the danger of snow avalanches with a machine learning approach using a comprehensive snow cover model. *Mach. Learn. Appl.* **2022**, *10*, 100405. [CrossRef]
25. Yu, W.; Li, X.; Zheng, L.; Zheng, L.; Zheng, L.; Kong, J.; Shao, Q.; Xiong, H.; Xie, C. Evaluation of the Susceptibility to Geological Hazards Based on the Information-Scoops3D Joint Model. *Disaster Prev. Mitig. Eng.* **2024**, *44*, 649–659. [CrossRef]
26. Chen, Q.; Liu, J.; Yang, Z.; Zhang, T.; Wang, B. Detection of avalanche spatial distribution and factors in the Arxiangou section of the Dukou Expressway. *Arid. Zone Res.* **2024**, *41*, 220–229. [CrossRef]
27. Li, Y.; Li, Y.; Zhao, Z. Assessment on Susceptibility of Debris Flow in Lushui Based on the Certain Factor Model. *Res. Soil Water Conserv.* **2019**, *26*, 336–342. [CrossRef]
28. Dou, J.; Oguchi, T.; Hayakawa, Y.S.; Uchiyama, S.; Paudel, U. GIS-based landslide susceptibility map using a certainty factor model and its validation in the Chuetsu Area, Central Japan. In *Landslide Science for a Safer Geoenvironment: Volume 2: Methods of Landslide Studies*; Springer International Publishing: Berlin/Heidelberg, Germany, 2014. [CrossRef]
29. Sujatha, E.R.; Rajamanickam, G.V.; Kumaravel, P. Landslide susceptibility analysis using Probabilistic Certainty Factor Approach: A case study on Tevankarai stream watershed, India. *J. Earth Syst. Sci.* **2012**, *121*, 1337–1350. [CrossRef]
30. Jia, W.; Wang, M. Influence Factors Analysis of Geological Disasters in Southeastern Tibet Based on Geographical Detector. In Proceedings of the IGARSS 2019-2019 IEEE International Geoscience and Remote Sensing Symposium, Yokohama, Japan, 28 July–2 August 2019; IEEE: Piscatvey, NJ, USA, 2019; pp. 3483–3486.

31. Liao, K.; Song, Y.; Xie, S.; Luo, Y.; Liu, Q.; Lin, H. Quantitative analysis of the factors influencing the spatial distribution of benggang landforms based on a geographical detector. *ISPRS Int. J. Geo-Inf.* **2022**, *11*, 337. [CrossRef]
32. Du, Y.; Ge, Y.; Liang, X.X.; Sun, Q.M.; Chen, P. Research of Debris Flow Susceptibility based on the Coupling of Certainty Factor Method and Geo Detector Model in Anning River Basin. *Disaster Prev. Mitig. Eng.* **2022**, *42*, 664–673. [CrossRef]
33. Wang, Q.; Xiong, J.; Cheng, W.; Cui, X.; Pang, Q.; Liu, J.; Chen, W.; Tang, H.; Song, N. Landslide Susceptibility Mapping Methods Coupling with Statistical Methods, Machine Learning Models and Clustering Algorithms. *J. Geo-Inf. Sci.* **2024**, *26*, 620–637.
34. Wang, Y.; Li, J.; Li, C.; Guo, M.; Hu, R.; Bao, A. 50 a Temporal and spatial variability of glacial lakes and their response to climate in the Bezin Tolgoi Mountains. *Arid Zone Res.* **2016**, *33*, 299–307. [CrossRef]
35. Li, Q. Comparative analysis of DEM ground curvature extraction based on different algorithms. *J. Cap. Norm. Univ. (Nat. Sci. Ed.)* **2016**, *37*, 82–85.
36. Li, Y.; Zhu, J.; Hu, Y.; Zhang, H. Comparative analysis of different interpolation methods simulating monthly precipitation in Sichuan Province. *Res. Soil Water Conserv.* **2017**, *24*, 151–154+160.
37. Wang, X.; Huang, P. Comparative study of meteorological element interpolation method based on ArcGIS. *Surv. Spat. Geogr. Inf.* **2020**, *43*, 167–170.
38. Jarvis, C.H.; Stuart, N. A comparison among strategies for interpolating maximum and minimum daily air temperatures. Part II: The interaction between number of guiding variables and the type of interpolation method. *Am. Meteorol. Soc.* **2001**, *40*, 1075–1084. [CrossRef]
39. Li, X.; Yang, S.; Li, Y.; Y, K.; Wang, W. Improved slope unit method for fine evaluation of regional landslide susceptibility. *Bull. Geol. Sci. Technol.* **2023**, *42*, 81–92. [CrossRef]
40. Huo, A.; Zhang, J.; Lu, Y.; Cheng, Y.C.; Yao, Y.L. Method of Classification for Susceptibility Evaluation Unit for Geological Hazards: A Case Study of Huang ling County, Shaanxi, China. *J. Jilin Univ. (Earth Sci. Ed.)* **2011**, *41*, 523–528+535. [CrossRef]
41. Gao, X.; Ma, P.; Lǔ, Y.; Zhao, J.; He, H. Geological Hazard Susceptibility Evaluation Based on a Statistical Method Coupled with Geographie Detector—A Casse Study Mountainous Area of Luliang City. *Bull. Soil Water Conserv.* **2024**, *44*, 193–205. [CrossRef]
42. Wu, K.; Su, W.; Ye, S.; Li, W.; Cao, Y.; Jia, Z. Analysis on the geographical pattern and driving force of traditional villages based on GIS and Geodetector: A case study of Guizhou, China. *Sci. Rep.* **2023**, *13*, 20659. [CrossRef]
43. Wu, Y.; Zhou, L.; Meng, Y.; Lin, Q.; Fei, Y. Influential Topographic Factor Identification of Soil Heavy Metals Using GeoDetector: The Effects of DEM Resolution and Pollution Sources. *Remote Sens.* **2023**, *15*, 4067. [CrossRef]
44. Liu, Y.; Chen, X.; Li, Q.; Yang, J.; Li, L.; Wang, T. Impact of different microphysics and cumulus parameterizations in WRF for heavy rainfall simulations in the central segment of the Tianshan Mountains, China. *Atmos. Res.* **2020**, *244*, 105052. [CrossRef]
45. Mock, C.J.; Kay, P.A. Avalanche Climatology of the Western United States, with an Emphasis on Alta, Utah. *Prof. Geogr.* **1992**, *44*, 307–318. [CrossRef]
46. Hao, J.-S.; Huang, F.-R.; Liu, Y.; Amanambu, A.C.; LI, L. Avalanche activity and characteristics of its triggering factors in the western Tianshan Mountains, China. *J. Mt. Sci.* **2018**, *15*, 1397–1411. [CrossRef]
47. Wen, L.; Xiang, L.; Cai, Y.; Su, F.; Yan, Z. Research on the formation mechanism of avalanches. *J. Mt. Sci.* **2016**, *34*, 1–11. [CrossRef]
48. Pei, Y.; Zhou, G.; Tian, X. Research on Urban Spatial Morphological Changes Based on GIS and RS—Taking Xichang City as an Example. *Bull. Surv. Mapp.* **2013**, *S2*, 217–221+229.
49. Zhu, Z.; Li, L.; Zhang, P.; Zhang, S.X.; Liang, Y.J.; Zhi, J.; Chen, Y. Influence of Vegetation Pattern on Microtopography and Erosion Under Hydraulic Erosion in Feldspathic Sandstone Region. *Res. Soil Water Conserv.* **2023**, *30*, 10–18+26. [CrossRef]
50. Li, L.; Qin, F.; Qian, Q.; Dong, X.Y.; Zhang, R.X.; Zhang, P. Micro-geomorphic Change Characteristics and Process of Slope Under Water Erosion in Pisha Sandstone Area. *Soils* **2022**, *54*, 198–205. [CrossRef]